ECS | The Electrochemical Society
Advancing solid state & electrochemical science & technology
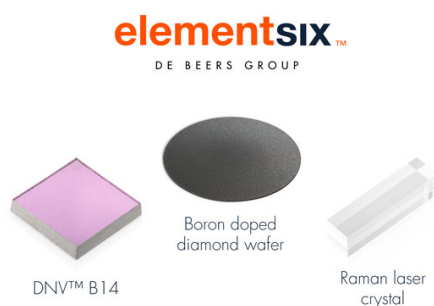
Applicability of Heat Generation Data in Determining the Degradation Mechanisms of Cylindrical Li-Ion Batteries

To cite this article: Kirill Murashko *et al* 2021 *J. Electrochem. Soc.* **168** 010511

View the article online for updates and enhancements.

Applicability of Heat Generation Data in Determining the Degradation Mechanisms of Cylindrical Li-Ion Batteries

Kirill Murashko,[1,*,z] **Dongjiang Li,**[2] **Dmitri L. Danilov,**[2,3] **Peter H. L. Notten,**[2,3] **Juha Pyrhönen,**[4] **and Jorma Jokiniemi**[1]

[1]*University of Eastern Finland, Kuopio Campus, Kuopio, FI-70211 Kuopio, Finland*
[2]*Institute of Energy and Climate Research (IEK-9), Forschungszentrum Jülich, Jülich, Germany*
[3]*Eindhoven University of Technology, 5600 MB Eindhoven, The Netherlands*
[4]*Lappeenranta-Lahti University of Technology LUT, 53850 Lappeenranta, Finland*

The applicability of heat generation data obtained after cylindrical Li-ion cells discharging with a constant current was analyzed thoroughly to determine cell degradation mechanisms. Different commercial and noncommercial cylindrical Li-ion cells, wherein graphite was used for negative electrode creation, were considered in this study and the degradation mechanisms were analyzed during cycling and storage. The heat generation in the cylindrical cells was estimated using heat flux and temperature measurements of the cell surface. The results obtained using analysis of the heat generation data were compared with those obtained using differential voltage analysis. The use of the heat generation data was shown to improve the detection and separation of the degradation mechanisms in Li-ion batteries during cycling and storage. The differential curve, which is based on the heat generation data, was proposed to investigate the degradation mechanisms. Moreover, the effects of the C-rate current and temperature on the form of the proposed differential curve were evaluated.

Rechargeable Li-ion batteries are currently considered the most suitable choice to power portable electronics, power tools, electrical vehicles, and various energy storage systems. These batteries have been widely used because of their significant advantages such as adequately high energy and power densities, long cycle life, low self-discharge rate, and negligible memory effect. However, to efficiently operate Li-ion batteries, a battery management system (BMS) is required, which should be capable of protecting these batteries from overcharging, overdischarging, and overheating. Moreover, the BMS should provide information about the degradation mechanisms of Li-ion batteries because changes in their operation characteristics strongly depend on the reason for battery aging.

The determination of the degradation mechanisms in Li-ion batteries is a difficult task because these batteries are non-linear and time-variable systems, whose internal electrochemical processes are nearly impossible to observe directly. Moreover, Li-ion battery degradation is typically caused by a combination of effects from different electrochemical processes, which further complicates the analysis of the degradation mechanisms.[1]

Many methods have been introduced to analyze the degradation of Li-ion batteries and to evaluate their state of health (SoH).[2] Among these methods, incremental capacity (IC) and differential voltage (DV) curve analyses have attracted tremendous attention because they can be used to investigate the degradation mechanisms and to estimate the SoH.[3–12] Moreover, these methods do not require intensive calculations, and they can be implemented on-board in the BMS.[13–15] Despite the advantages of the IC and DV curve analyses, they have disadvantages that may limit their application. A constant temperature and a low constant current are required in differential curve measurements.[16] Moreover, the DV and IC curves are obtained on the basis of the terminal voltage of the Li-ion batteries. However, in the majority of these battery chemistries, terminal voltage is mostly determined by the positive electrode potential; therefore, changes in the negative electrode potential related to battery degradation are difficult to discern.[16] These disadvantages may render it impossible to detect some of the degradation mechanisms in Li-ion batteries. Therefore, the existing methods

based on differential curve analysis have to be modified to improve their applicability. Recently, the DV curve analysis was modified by considering the measured heat flux and temperature data with the commonly measured terminal voltage and current.[17,18] These studies showed that the consideration of the heat generation data, which were obtained by measuring the heat flux and temperature of the cylindrical Li-ion cell surface, allowed a decrease in the effect of the C-rate current on the position and amplitude of the important peaks of the differential curves. Moreover, these modified differential curves provided information about the change in entropy (ΔS) during Li-ion battery aging.[17,18] However, the possibility of using the information regarding ΔS to improve the determination of the degradation mechanisms in cylindrical Li-ion batteries has not been explored.

The aim of this study was to provide a detailed analysis of the applicability of heat generation data to determine the degradation mechanisms in Li-ion batteries. The change in ΔS with the aging of Li-ion cells, which can be obtained from the measured heat flux and temperature data, was investigated to elucidate the determination of the degradation mechanisms. The accuracy of the ΔS measurements was confirmed by comparing the obtained results with the ΔS results measured by applying commonly used methods at different states of charge (SoCs).

Materials and methods

Test setup.—Cylindrical Li-ion cells with the most widely studied chemistries were selected for the analysis. The characteristics of the selected cylindrical Li-ion cells are listed in Table I. A Neware battery tester (CT-4008-5V6A-S1) was used for charging and discharging. Cell cycling and measurements of cell operation characteristics were performed in metallic chambers with a liquid jacket, where the temperature of the liquid was controlled by using refrigerated/heating circulators (JULABO F25-HE). The terminal voltage and current in all the tests were measured using the battery tester. The temperature of the cylindrical cell surface and the heat flux from this surface were measured using a PT100 temperature sensor and a heat flux sensor (gSKIN® XM 26 9 C), respectively. These sensors were installed on the cylindrical cell surface in the middle of the cell, similar to protocols in other studies.[17,18,19] A data logger (Pico Technology PT104 RTD) was used to record the temperature and heat flux. A protocol from a previous study[19] was

*Electrochemical Society Member.
zE-mail: kirill.murashko@uef.fi

Table I. Parameters of the cylindrical Li-ion cells.

Name of the cell	Chemistry	Capacity, Ah	Mass, g	Dimensions (diameter/length), mm
ANR26650M1B	Lithium iron phosphate/graphite (LFP/G)	2.5	70	25.85/65.15
INR26650EC	Lithium nickel manganese cobalt oxide /graphite (NMC/G)	4.4	82	26.2/65.0
NCR18650PF	Lithium nickel cobalt aluminum oxide/graphite (NCA/G)	2.7	48	18.5/65.3
LR1865HB (non-commercial)	Lithium nickel cobalt aluminum oxide /(silicon/graphite) (NCA/SiG)	3.1	48.5	18.65/65.15

Table II. Aging test parameters.

Chemistry	Discharging cut-off voltage, V	Charging cut-off voltage, V	Discharging/charging C-rate current	Total number of cycles
LFP/G	1.6	3.6	2/2	2548
NMC /G	3.0	4.2	1/1	251
NCA/G	2.5	4.2	1/0.5	643
NCA/SiG	2.7	4.2	1/0.5	191

used to thermally isolate the tabs of the cylindrical cells by using extruded polystyrene foam, which allowed to simplify heat generation calculations.

Aging protocol.—The aging of the Li-ion cylindrical cells under consideration was performed to evaluate the changes in operation characteristics during degradation. The aging test was divided into two parts. In the first part, the Li-ion cylindrical cells were cycled at 45 °C. The cells were fully charged initially using the constant current (CC) mode up to the cut-off charging voltage, followed by the constant voltage (CV) mode. The charging of the cells in the CV mode was finished after fulfilling one of two conditions: the charging current decreased below the 0.1 C-rate or the charging time in the CV mode was >2 h. Furthermore, cells were discharged in the CC mode down to the cut-off discharging voltage. The values of the charge–discharge C-rate currents were chosen in an operation diapason recommended by the battery manufacturers. A 30 min relaxation time between discharging and charging was considered in all the experiments. This cell operation protocol was continued until the cell capacity decreased by ~15%. The characterization of the Li-ion cells was performed whenever the capacity of the cells decreased by ~5%. When the capacity decreased by >15% from the initial value, the second part of the aging test was applied. Fully charged Li-ion cells were stored at 45 °C for approximately three months and subsequently cycled again (similar to the first part of the aging test) until the capacity decreased by >20% from the initial value. This deviation in the aging tests was considered to facilitate the analysis of different degradation mechanisms, which are categorized into the following three degradation modes:[20] loss of the active material of the negative electrode (LAM_NE), loss of the active material of the positive electrode (LAM_PE), and loss of the lithium inventory (LLI). It was previously reported by other researchers[21,22] that LAM_NE and LAM_PE must be the dominant degradation modes during cycling, and the storage of Li-ion cells should accelerate LLI. Additional information about the aging test parameters is given in Table II.

Characterization of Li-ion cells.—The DV and open-circuit voltage (OCV) curves were measured during the degradation of the Li-ion cells using approaches similar to those in a previous work.[18] DV curves were measured during cell discharging by using a 1/2 C-rate current for the LFP/G cell and a 1/4 C-rate current for all other Li-ion cells. Different values of the C-rate current were used for these cells because LFP/G is a high-power Li-ion cell, whereas the others are high-energy Li-ion cells. The DV curves were measured at different temperatures with 10 °C step from 5 °C to 45 °C. C-rate currents of 0.1, 0.15, 0.2, and 0.25 were used during discharging of the cylindrical Li-ion cells for the OCV curve extrapolation, by using a protocol similar to the one reported in a previous study.[18] Entropy change (ΔS) was measured using a potentiometric method and a method reported previously,[19] at every increment of 10% in the SoC from 10% to 90%. Discharging of the cells to achieve a new value of SoC was performed in the CC mode with a 1 C-rate current for the LFP/G cell and with a 1/4 C-rate current for all other cells. The thermal parameters of the cylindrical cell, such as heat capacity and thermal conductivity, were measured using a method reported in a previous study.[23] The OCV and thermal parameters of the Li-ion cells were measured at 25 °C. The dependence of the thermal parameters on the SoC was considered in this analysis. However, the temperature dependence of the thermal

parameters was neglected to simplify the heat generation calculations. The thermal parameters were estimated at 0, 50, and 100% SoC, and the temperature of the cell was varied between 23 °C and 60 °C. The modified DV curves were obtained from the measured heat generation data by using a method presented in previous studies.[17,18] Heat generated Q [W] during cell discharging at each point in time was calculated as

$$\int_{t_0}^{t_{\text{end}}} \dot{Q}(t)\,dt = \frac{V}{a} \cdot (k \cdot (T - T_0) + r \cdot \boldsymbol{\theta} \times \mathbf{S}) \quad [1]$$

where V [m^3] is the volume of the cylindrical cell, T [K] is the temperature on the cylindrical cell surface, T_0 [K] is the initial temperature of the cylindrical cell surface, a [m^2/s] is the thermal diffusivity, k [W/(m K)] is the through-plane thermal conductivity, and r [m] is the radius of the cylindrical cell. Matrices $\boldsymbol{\theta}$ and $\mathbf{S}$ include the temperature coefficients and heat flux data, respectively. The method for creating these matrices is reported in a previous study.[19] The thermal diffusivity is calculated using

$$a = \frac{k}{\rho \cdot C_{\text{th}}} \quad [2]$$

where ρ [kg/m^3] is the density of the Li-ion cell and C_{th} [J/(kg K)] is the heat capacity.

The modification of the DV curve analysis method was carried out by considering a simplified form of the heat equation presented by Bernardi,[24] in which the phase change and mixing effects were neglected. The simplified form of the heat equation is as follows:

$$\dot{Q} = I \cdot \left(U_{\text{ocv}} - U - T \cdot \frac{\partial U_{\text{ocv}}}{\partial T} \right) \quad [3]$$

where I [A] is the discharging current (which has a positive value during discharging), U [V] is the terminal voltage, and U_{ocv} [V] is the OCV. Modification of Eq. 3 gives the following equation for the differential curve using an approach similar to the DV curve analysis method:

$$-\frac{\partial(\dot{Q}/I + U)}{\partial Q} = -\frac{\partial U_{\text{ocv}}}{\partial Q} + \frac{\partial\left(T \cdot \frac{\Delta S}{n \cdot F}\right)}{\partial Q} =$$
$$-\frac{\partial U_{\text{ocv}}}{\partial Q} + \frac{T}{n \cdot F}\frac{\partial(\Delta S)}{\partial Q} + \frac{\Delta S}{n \cdot F}\frac{\partial(T)}{\partial Q} \quad [4]$$

where ΔS [J/(mol K)] is the entropy change, F is the Faraday constant ($F = 96485$ C mol^{-1}), and n is the stoichiometric number of electrons participating in the cell reaction ($n = 1$ for a Li-ion cell).

The effects of the current and temperature on the key features of the differential curves were investigated using 1/3, 1/2, 1, 3/2, and 2 C-rate currents for the LFP/G cell and 1/4, 1/3, 1/2, and 2/3 C-rate currents for all other cells. Discharging of the Li-ion cells was performed at different temperatures from 5 °C to 45 °C with increments of 10 °C in between.

Results and Discussion

The measured OCV curves for all the cells under consideration before starting the aging tests are shown in Fig. 1. The maximum
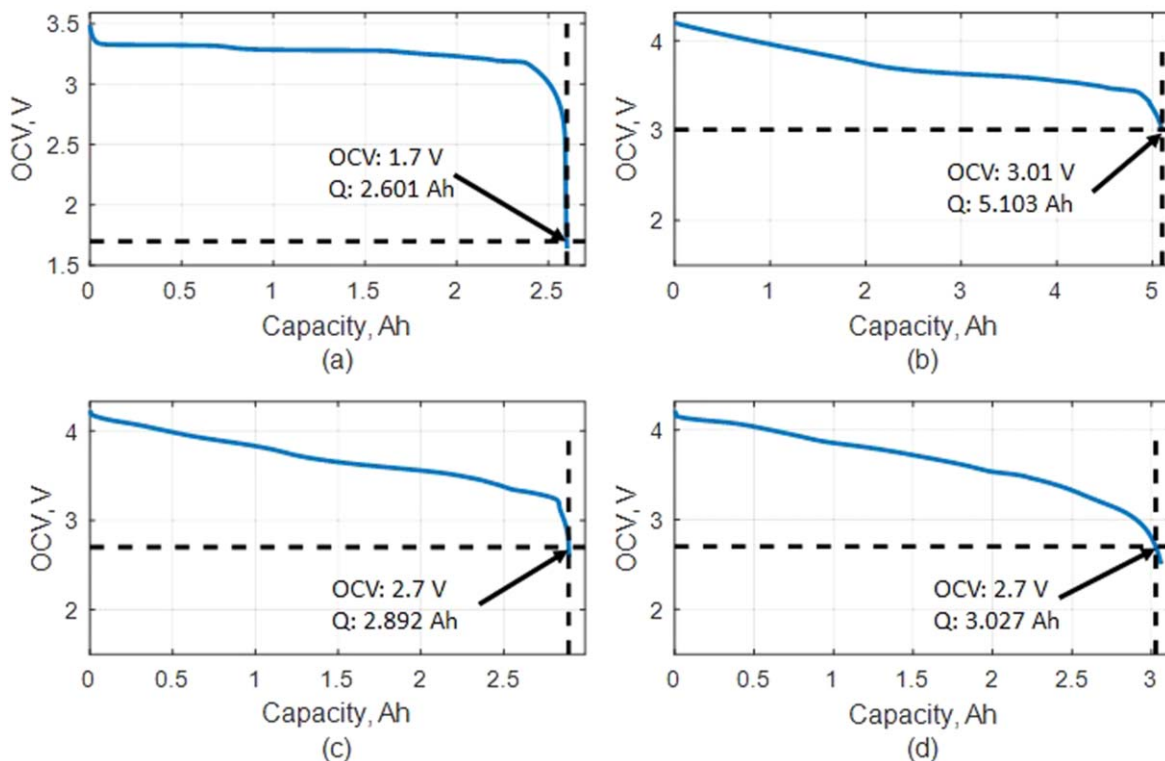
Figure 1. Extrapolated OCV curves of LFP/G cell (a), NMC/G cell (b), NCA/G cell (c) and NCA/SiG cell (d).

capacity of the cylindrical cells was obtained from the measured OCV curves when the OCV decreased below the selected values, as shown in Fig. 1. These OCV values were further used to determine the maximum capacity of the Li-ion cells at different stages of their aging.

The degradation mechanisms in the cylindrical Li-ion cells during cycling and storage were analyzed by using an approach similar to the DV analysis method, by considering the changes in the features of the $\partial U_{OCV}/\partial Q$ curves during Li-ion cell aging. The $\partial U_{OCV}/\partial Q$ curves as a function of SoC are shown in Fig. 2. Each subsequent curve was shifted upward by 0.3 V/(A h) from the previous one to improve the visibility of the key features of the differential curve at different aging stages. The vertical step of the grid in Fig. 2 is 0.5 V/(A h).

The differential curve analysis showed that the predominant degradation mechanism for all the cells during the first part of the aging tests was LAM_{NE} as the positions of the key features of the differential curves, presented as function of SoC, did not change significantly during Li-ion cell degradation. Such effect of LAM_{NE} was also reported by other researchers previously.[21] LAM_{PE} was also noticeable during NCA/G and NMC/G cell aging, which led to smoothing of peak α after the cells were cycled. Peak α belongs to the positive electrode and disappears if the amount of useful active material on the positive electrode decreases.[21]

The LLI in the first part of the aging tests was slightly detectable during NCA/SiG cell cycling [Fig. 2d], which led to the movement of γ and β peaks to higher values of SoC. LLI was slightly detectable only in the case of the NCA/SiG cell in the first part of aging tests, because the addition of silicon to the graphite anode can accelerate the LLI degradation mode, as reported previously.[25,26] However, for the other Li-ion cells under consideration, the LLI degradation mechanisms should be accelerated during high-temperature storage.[22] Therefore, it was expected that in the second part of the aging test, LLI should be easily detected in all the Li-ion cells under consideration. However, a significant LLI could only was detected in the LFP/G and NCA/SiG cells after the second part of the aging tests, during which the cells were initially stored at 45 °C and cycled

subsequently. In the case of the NMC/G and NCA/G cells, the disappearance of peak α, caused by LAM_{PE}, complicated the investigation of the degradation mechanisms because only one differential curve peak was visible.

The modified DV curve analysis method[17,18] was proposed to improve the determination of degradation mechanisms during cell aging. Thermal parameters of the Li-ion cells, such as specific heat capacity and through-plane thermal conductivity, were measured before starting the aging tests, using a method presented in a previous work[23] at different values of SoC. An analysis of the effects of SoC on the thermal parameters of the cylindrical Li-ion cells, shown in Fig. 3, allowed us to assume a linear dependence between them. This dependence was considered in the determination of heat generation and the ΔS curves using the following equations:

$$C_{th} = a_1 \cdot SoC + a_2 \quad [5]$$

$$k = b_1 \cdot SoC + b_2 \quad [6]$$

where a_i and b_i are fitting constants ($i = 1$ and 2), and SoC is the state of charge, which varies from 0 to 1. The fitting constants obtained from the measured data are listed in Table III for all the cylindrical Li-ion cells under consideration.

The modified DV curves were obtained using Eq. 4 after the Li-ion cells were discharged using 1/2 and 1/4 C-rate current for the LFP/G cell and all other Li-ion cells under consideration, respectively. As in the case of the $\partial U_{OCV}/\partial Q$ curves, the modified DV curves are presented in Fig. 4 as a function of SoC. Each subsequent

Table III. Fitting constants.

Chemistry	a_1	a_2	b_1	b_2
LFP/G	28	1124.7	−0.0212	0.4686
NMC /G	62	1282.7	−0.0372	0.5587
NCA/G	21.3	826.4	0.1942	0.6661
NCA/SiG	61	1027.2	0.2481	0.6299
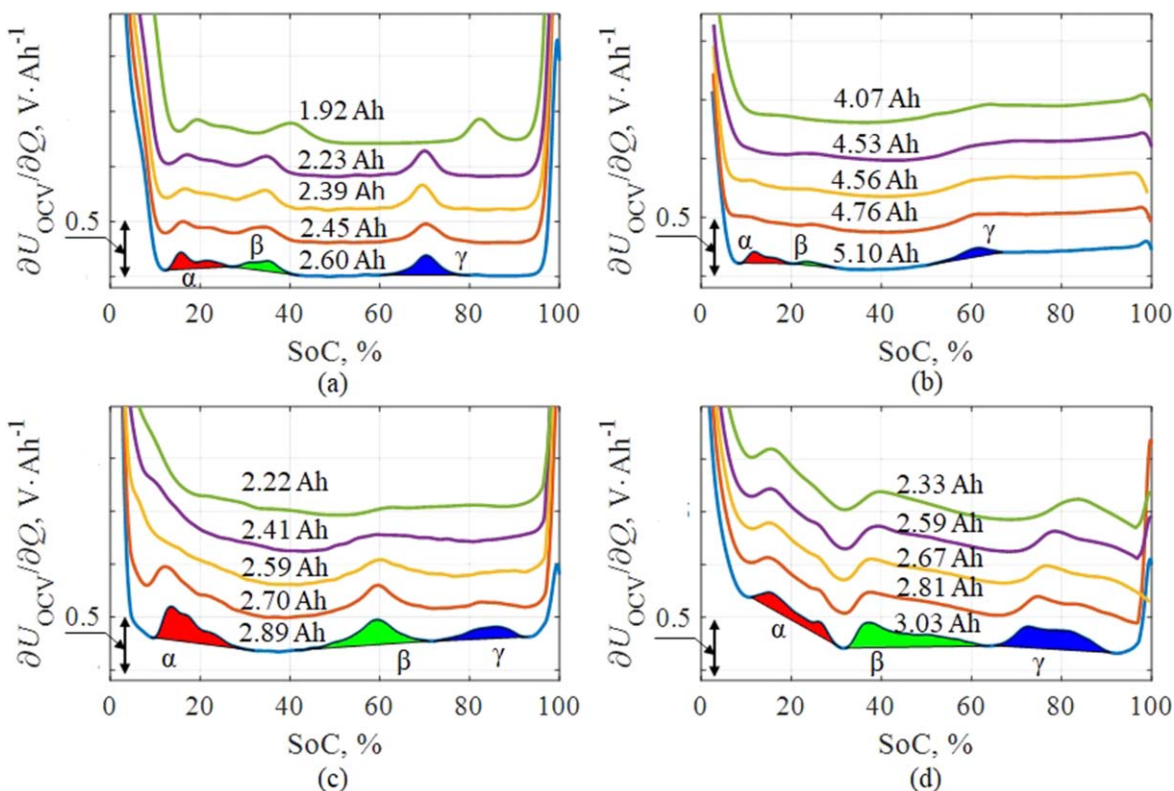
Figure 2. $\partial U_{OCV}/\partial Q$ curves as a function of the SoC at different aging stages of LFP/G cell (a), NMC/G cell (b), NCA/G cell (c) and NCA/SiG cell (d). As the curves are sifted to different levels for readability only the part of the *y*-axis is given.
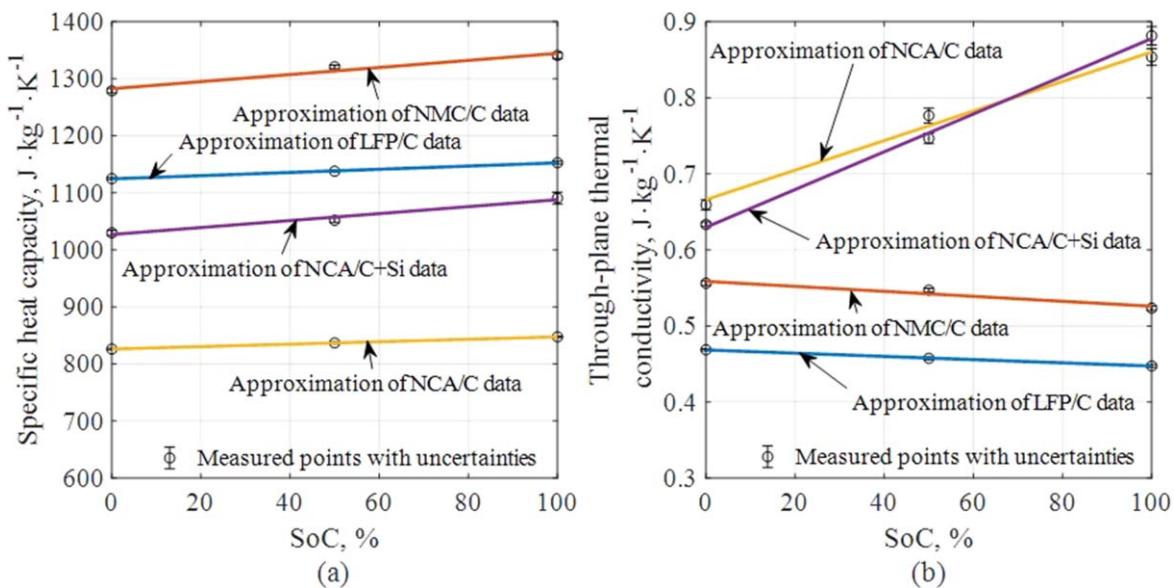

Figure 3. Analysis of the SoC effect on the specific heat capacity of the cylindrical Li-ion cells (a) and through-plane thermal conductivity (b).

curve was shifted upward by 0.5 V/(A h) from the previous one to improve the visibility of the key features of the differential curve at different aging stages. The vertical step of the grid in Fig. 4 is 1 V/(A h).

The suggested modification of the DV curve[17,18] provides nearly the same information about the degradation mechanisms, which can be obtained by considering the $\partial U_{OCV}/\partial Q$ curves. The negative peak δ, which is visible in all the modified DV curves, is caused by the effect of the $(T/(n \cdot F)) \cdot \partial(\Delta S)/\partial Q$ term in Eq. 4. In addition, these modified DV curves were obtained during cell discharging by a

relatively high current, which is considered a significant advantage of this method. Unfortunately, as seen in Fig. 4, the peaks of the modified DV curves are also smoothed with cell aging, similar to those found during the $\partial U_{OCV}/\partial Q$ curve analysis; this complicated the determination of the degradation mechanisms with further battery aging. This was especially noticeable for the NMC/G and NCA/G cells, wherein the expected degradation mechanisms associated with the LLI mode could not be detected after the second part of the aging tests because of the disappearance of the differential curve peaks. Moreover, because the modified differential curves
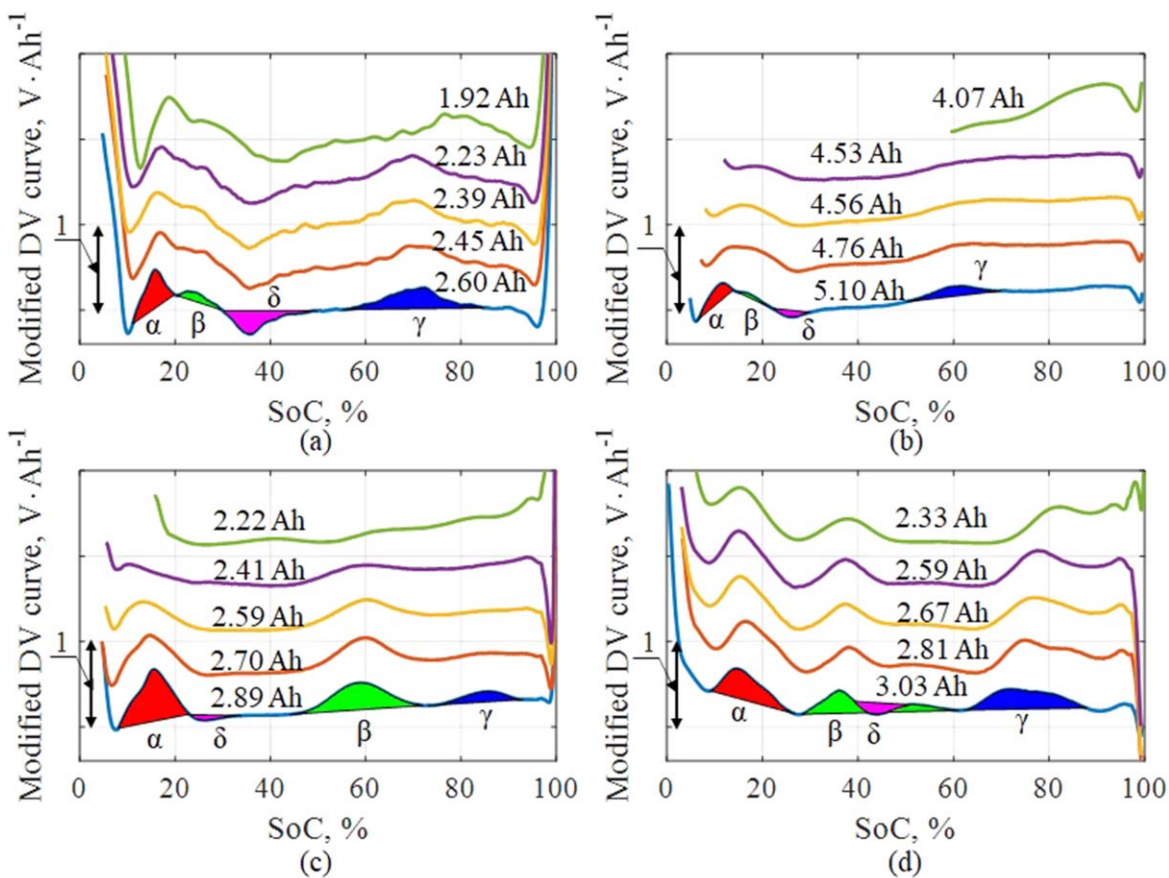
Figure 4. Modified DV curves at different aging stages of LFP/G cell (a), NMC/G cell (b), NCA/G cell (c) and NCA/SiG cell (d). As the curves are shifted to different levels for readability only the part of the *y*-axis is given.

were obtained after discharging the Li-ion cells using a relatively high C-rate current (1/2 C-rate for the LFP/G cell and 1/4 C-rate for all other cells), the internal resistance of these cells has an effect on the minimum value of the SoC, which can be reached during discharging in the CC mode. This was seen in the NMC/G cell, wherein the internal resistance increased significantly during the last part of the aging test. Therefore, full discharging of the NMC/G cell could not be performed using a high C-rate current because of the minimum terminal voltage limitation.

The effect of ΔS on the heat generated during the discharging of the cells was considered to find a solution to the problems described above. ΔS curves as a function of the SoC were measured using the potentiometric method. ΔS curves, modified DV curves, differential OCV curves ($\partial U_{OCV}/\partial Q$), and $(T/(n \cdot F)) \cdot \partial(\Delta S)/\partial Q$ curves are presented in Fig. 5 as a function of SoC to analyze the effects of the different terms of Eq. 4 on the key features of the modified DV curves. The last term in Eq. 4 was not considered in this analysis because its effect on the modified DV curves was negligible. The $(T/(n \cdot F)) \cdot \partial(\Delta S)/\partial Q$ curves were plotted using ΔS data measured by the potentiometric method.

The data presented in Fig. 5 show a noticeable dependence between the change in ΔS during cell discharging and the lithium deintercalation stages from graphite. A significant change in ΔS can be seen at each stage of graphite delithiation, which was also reported by other researchers.[27] Therefore, the graphite delithiation stage could be defined by considering the $(T/(n \cdot F)) \cdot \partial(\Delta S)/\partial Q$ curve. However, because the modified DV curve also included information about the $\partial U_{OCV}/\partial Q$ curve, the effects of the $(T/(n \cdot F)) \cdot \partial(\Delta S)/\partial Q$ curve were not easily discernible in the analysis of the modified DV curves, which can be seen in the Li-ion cells with NMC and NCA positive electrodes. The visibility of the $(T/(n \cdot F)) \cdot \partial(\Delta S)/\partial Q$ curve features can be improved by

considering the overpotential (η) instead of the OCV in Eq. 4. In this case, the differential curve is described by the following equation:

$$-\frac{\partial(\dot{Q}/I)}{\partial Q} = -\frac{\partial \eta}{\partial Q} + \frac{T}{n \cdot F}\frac{\partial(\Delta S)}{\partial Q} + \frac{\Delta S}{n \cdot F}\frac{\partial(T)}{\partial Q} \qquad [7]$$

The decision to improve the visibility of the $(T/(n \cdot F)) \cdot \partial(\Delta S)/\partial Q$ curve features was made by assuming that the change in overpotential, during cell discharging under normal operating conditions, is significant only at the beginning and end of discharging. The differential curve presented in Eq. 7 can be easily obtained using the same data that are required to obtain the modified DV curve. To confirm this assumption, the $-\partial(\dot{Q}/I)/\partial Q$ and $(T/(n \cdot F)) \cdot \partial(\Delta S)/\partial Q$ curves were compared (Fig. 5). The comparison showed that the difference between these curves, presented as a function of SoC, is quite small and is mostly caused by a large increment in the SoC ($\sim$10%), which was used to determine ΔS using the potentiometric method. Moreover, because the overpotential depends significantly on the C-rate current and temperature, an analysis of the effects of the C-rate current and temperature on the key feature positions of the $-\partial(\dot{Q}/I)/\partial Q$ curves was performed on the basis of the high-power LFP/G and high-energy NMC/G cells (Fig. 6). Analyze of the effect of the C-rate current on the positions of the key peaks of the differential curves showed that an increase in the current may led to the smoothing of the key features of the differential curves. This effect was more noticeable at the end of the discharging tests, which allowed us to assume that it was likely caused by an increase in the Li-ion concentration gradient during the increase in the C-rate current. The effect of temperature on the key features of the differential curves
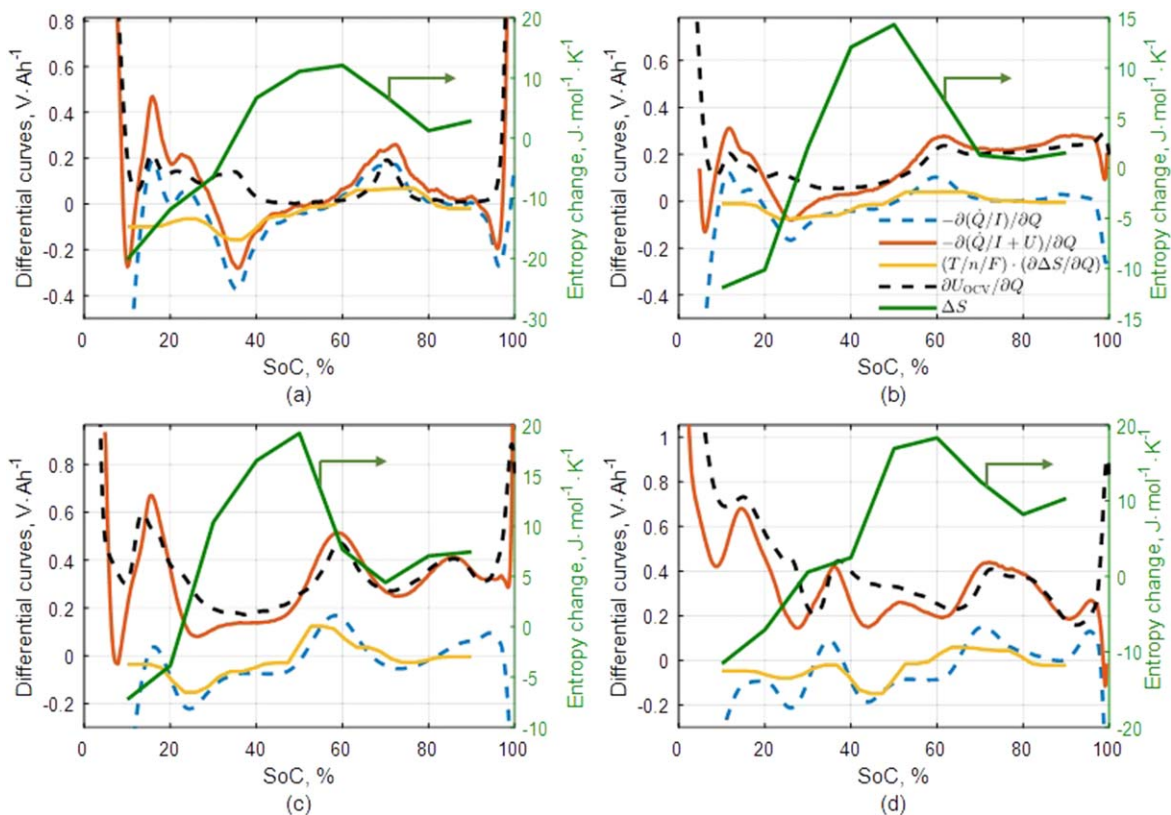
Figure 5. Differential curves and ΔS curves as functions of the SoC of LFP/G cell (a), NMC/G cell (b), NCA/G cell (c) and NCA/SiG cell (d) at the beginning of aging tests.
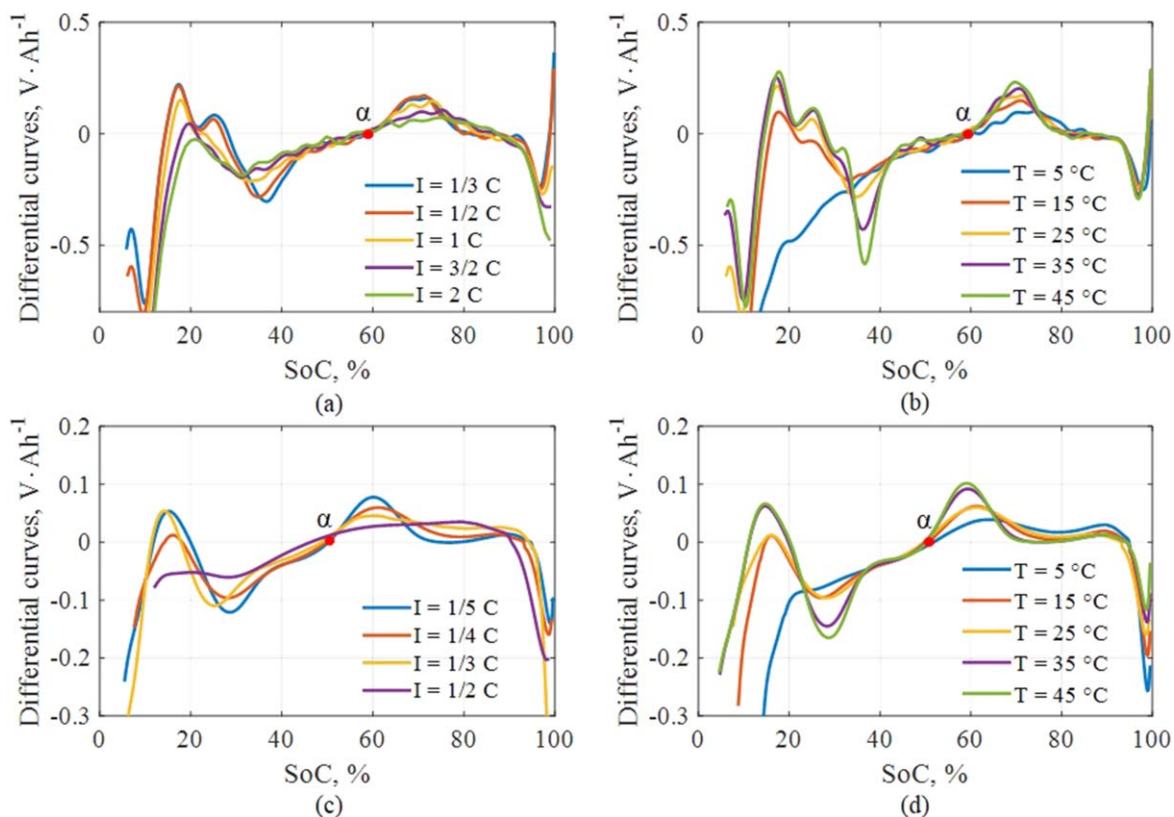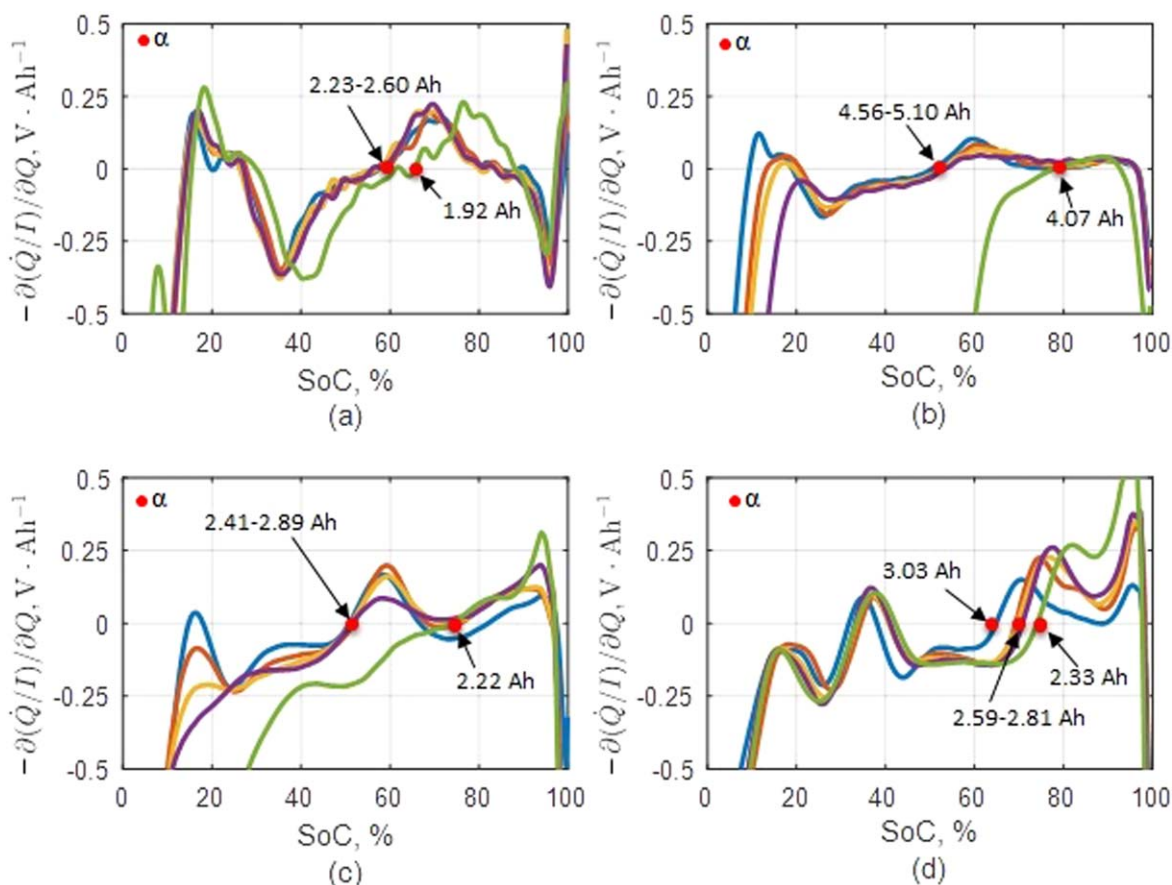

Figure 6. $-\partial(\dot{Q}/I)/\partial Q$ curves of LFP/G and NMC/G cells at different C-rate currents (a) and (c) and temperature (b) and (d), correspondingly.

can also be associated with an increase in the Li-ion concentration gradient when the temperature decreased, which also led to smoothing of these key features. It should be noted that no significant effects of the temperature and current were observed on the differential curve features approximately in the middle of the SoC, when the differential curves cross the horizontal axis (the point denoted as α). The α corresponds to the maximum value of ΔS in the second stage of the graphite delithiation (LiC_{12}). The consideration of the point where the differential curves crossed the horizontal axis, during the evaluation of the degradation mechanisms could allow the determination of the ΔS curve peak shift along the horizontal axis, which should occur during the LLI. The positions of α on the $-\partial(\dot{Q}/I)/\partial Q$ curve measured at different aging stages of the cylindrical Li-ion cells were analyzed to confirm the assumption made. These differential curves are presented in Fig. 7 as a function of the SoC. Moreover, the effects of the different predominant degradation mechanisms on the ΔS curves were analyzed to confirm the shift of the ΔS curves during LLI in all the Li-ion cells under consideration. The entropy change was measured as a function of the SoC at each stage of the Li-ion cell aging by using the potentiometric method and a method based on the heat flux measurements presented in a previous study.[19] The ΔS curves were obtained using the potentiometric method only at the beginning and the end of the aging tests, because this method was very time consuming. Another method, which is based on heat flux measurements,[19] was used in the ΔS measurements at all characterization points. Each subsequent ΔS curve was shifted upward by 10 J/(mol K) from the previous one to improve the visibility of these curves, as shown in Fig. 8. The vertical step of the grid in Fig. 8 is 20 J/(mol K). As seen in Fig. 7, the differential curves measured for the LFP/G, NMC/G, and NCA/G cells during the first part of the aging tests cross the horizontal axis at approximately the same SoC,

which allowed us to conclude that the degradation mechanisms associated with the LLI degradation mode were not significant in this part of the aging tests. This was also confirmed by the $\partial U_{OCV}/\partial Q$ curve analysis and the ΔS measurements (Figs. 8a–8c). For the NCA/SiG cell, a significant movement of the point α was observed on the $-\partial(\dot{Q}/I)/\partial Q$ curve at the beginning of the cycling. With aging of this cell, a shift of the point α was also observed, however, it was very small. This shift of the ΔS curve to the right was also confirmed during the ΔS measurement (Fig. 8d). The deviation in the aging of the NCA/SiG cells from the aging of all other Li-ion cells was likely caused by the addition of silicon to the graphite negative electrode. The high-volume changes in the silicon during lithium intercalation led to a partial destruction of the solid–electrolyte interface (SEI) and lithium consumption during SEI recovery. The smoothing of the $-\partial(\dot{Q}/I)/\partial Q$ curves in the NMC/G and NCA/G cells at low values of SoC was likely caused by the LAM_{PE}; this was shown in the analysis of the degradation mechanisms in these cylindrical Li-ion cells using the $\partial U_{OCV}/\partial Q$ curves (Fig. 4).

After all aging tests, the shift of the point α that corresponds to the maximum value of ΔS, and at which the differential curves cross the horizontal axis, was observed for all the Li-ion cells under consideration, which confirms the assumption regarding the applicability of the proposed differential curves for the determination of LLI during the Li-ion cell aging. Moreover, the shift of the measured ΔS curves to higher values of SoC was also observed. Therefore, it can be concluded that the degradation of the Li-ion cells in the second part of the aging tests was partly caused by LLI in all the Li-ion cells that were studied. Because of the shown possibility of the proposed differential curve (Eq. 7) to determine the degradation mechanisms with higher accuracy that differential voltage curve, the use of this differential curve separately or in combination with the

Figure 7. $-\partial(\dot{Q}/I)/\partial Q$ curves at different aging stages of LFP/G cell (a), NMC/G cell (b), NCA/G cell (c) and NCA/SiG cell (d).
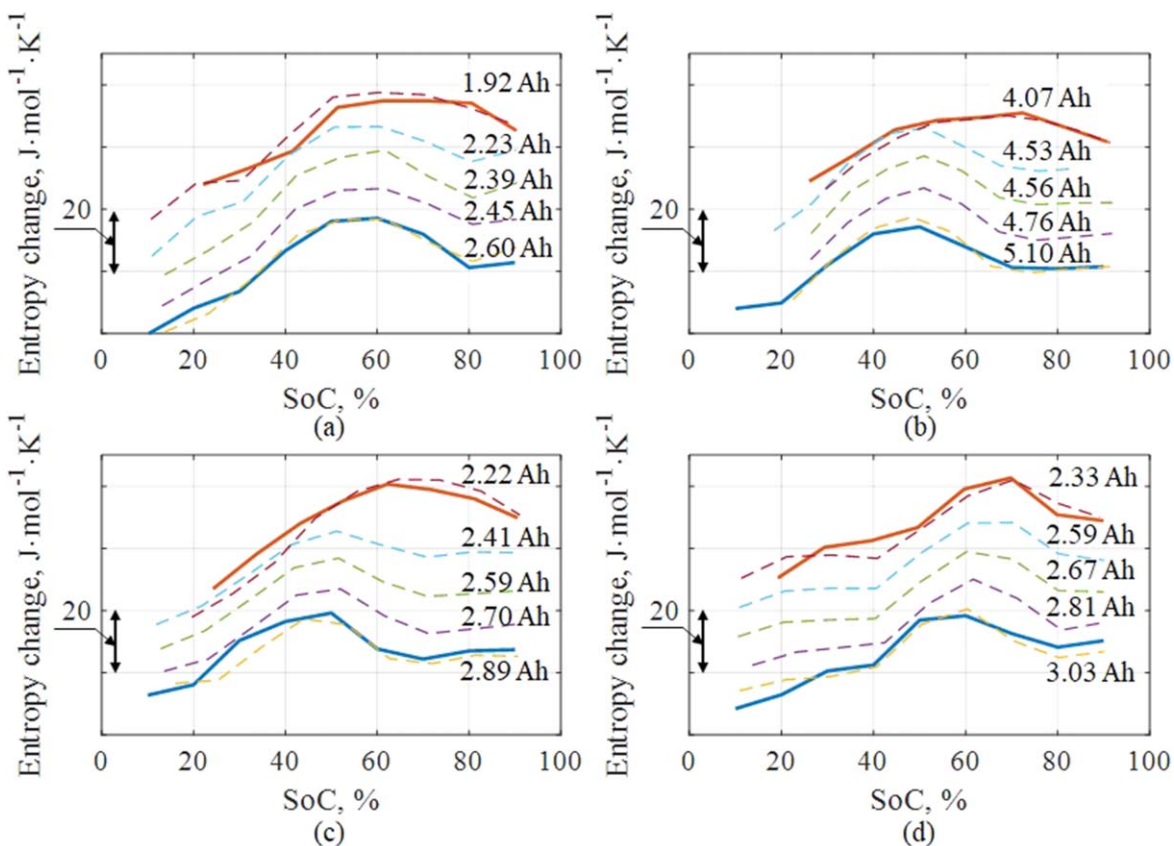
Figure 8. Entropy change at different aging stages of LFP/G cell (a), NMC/G cell (b), NCA/G cell (c) and NCA/SiG cell (d) measured by potentiometric method (solid line) and by the method presented in Ref. (dashed line). As the curves are sifted to different levels for readability only the part of the *y*-axis is given.

modified DV curve, is recommended to increase the accuracy of the determination of the degradation mechanisms during Li-ion battery aging.

Conclusions

The applicability of heat generation data that were obtained using heat flux and temperature measurements on the surface of cylindrical Li-ion cells, for the analysis of the degradation mechanisms occurring in these cells during their operation was analyzed in detail. Different commercial and noncommercial cylindrical Li-ion cells with graphite negative electrodes were considered in the analysis. It was shown that at the end of the battery life, significant deformation and disappearance of the key features of the $\partial U_{\text{OCV}}/\partial Q$ curve may complicate the identification and separation of the degradation mechanisms. However, consideration of heat generation in the Li-ion cells during their aging improved the accuracy of the degradation mechanism determination even in case when a relatively high C-rate current was used for the differential curve measurement. The accuracy was improved by considering the shift of the ΔS curve caused by battery degradation associated with the LLI mode. To confirm this effect, the maximum value of the ΔS curve, which was mainly determined by the entropy change in the graphite negative electrode, was selected as the key feature and its position was analyzed during the Li-ion battery aging. The analysis showed that a shift of this key feature during aging associated with the LLI mode. Moreover, the differential curve, which was obtained using heat generation data, reflected the behavior of the selected key feature on the ΔS curve and was, therefore, proposed for detection of the battery degradation associated with the LLI mode. Further analysis showed a negligible effect of the C-rate current and the temperature on the visibility of the key feature of the proposed differential curve. Therefore, the use of the proposed differential curve, separately or in

combination with the modified DV curve, was recommended to increase the accuracy of the degradation mechanism determination during Li-ion battery aging.

ORCID

Kirill Murashko https://orcid.org/0000-0003-0177-8503

References

1. J. Vetter, P. Novák, M. R. Wagner, C. Veit, K.-C. Möller, J. O. Besenhard, M. Winter, M. Wohlfahrt-Mehrens, C. Vogler, and A. Hammouche, *J. Power Sources*, **147**, 269 (2005).
2. M. Berecibar, I. Gandiaga, I. Villarreal, N. Omar, J. Van Mierlo, and P. Van den Bossche, *Renew. Sustain. Energy Rev.*, **56**, 572 (2016).
3. I. Bloom, J. Christophersen, and K. Gering, *J. Power Sources*, **139**, 304 (2005).
4. I. Bloom, J. P. Christophersen, D. P. Abraham, and K. L. Gering, *J. Power Sources*, **157**, 537 (2006).
5. I. Bloom, A. N. Jansen, D. P. Abraham, J. Knuth, S. A. Jones, V. S. Battaglia, and G. L. Henriksen, *J. Power Sources*, **139**, 295 (2005).
6. D. Li, D. L. Danilov, L. Gao, Y. Yang, and P. H. L. Notten, *Electrochim. Acta*, **210**, 445 (2016).
7. D. Li, H. Li, D. Danilov, L. Gao, J. Zhou, R.-A. Eichel, Y. Yang, and P. H. L. Notten, *J. Power Sources*, **396**, 444 (2018).
8. M. Dubarry, C. Truchot, B. Y. Liaw, K. Gering, S. Sazhin, D. Jamison, and C. Michelbacher, *J. Power Sources*, **196**, 10336 (2011).
9. D. Anseán, M. Dubarry, A. Devie, B. Y. Liaw, V. M. García, J. C. Viera, and M. González, *J. Power Sources*, **321**, 201 (2016).
10. M. Ouyang, D. Ren, L. Lu, J. Li, X. Feng, X. Han, and G. Liu, *J. Power Sources*, **279**, 626 (2015).
11. A. Devie, M. Dubarry, and B. Y. Liaw, *J. Electrochem. Soc.*, **162**, A1033 (2015).
12. M. Dubarry, C. Truchot, and B. Y. Liaw, *J. Power Sources*, **258**, 408 (2014).

13. Y. Li, M. Abdel-Monem, R. Gopalakrishnan, M. Berecibar, E. Nanini-Maury, N. Omar, P. van den Bossche, and J. Van Mierlo, *J. Power Sources*, **373**, 40 (2018).
14. T. Goh, M. Park, M. Seo, J. G. Kim, and S. W. Kim, *Energy*, **135**, 257 (2017).
15. C. Pastor-Fernández, K. Uddin, G. H. Chouchelamane, W. D. Widanage, and J. Marco, *J. Power Sources*, **360**, 301 (2017).
16. B. Wu, V. Yufit, Y. Merla, R. F. Martinez-Botas, N. P. Brandon, and G. J. Offer, *J. Power Sources*, **273**, 495 (2015).
17. K. Murashko, D. Li, D. L. Danilov, P. H. L. Notten, J. Pyrhonen, and J. Jokiniemi, *2019 IEEE Vehicle Power and Propulsion Conference (VPPC), IEEE*, p. 1 (2019).
18. K. A. Murashko, A. V. Mityakov, V. Y. Mityakov, S. Z. Sapozhnikov, J. Pyrhönen, and J. Jokiniemi, *J. Electrochem. Soc.*, **166**, A2896 (2019).
19. K. A. Murashko, A. V. Mityakov, V. Y. Mityakov, S. Z. Sapozhnikov, J. Jokiniemi, and J. Pyrhönen, *J. Power Sources*, **330**, 61 (2016).
20. C. R. Birkl, M. R. Roberts, E. McTurk, P. G. Bruce, and D. A. Howey, *J. Power Sources*, **341**, 373 (2017).
21. M. Dubarry, C. Truchot, and B. Y. Liaw, *J. Power Sources*, **219**, 204 (2012).
22. T. Waldmann, M. Wilka, M. Kasper, M. Fleischhammer, and M. Wohlfahrt-Mehrens, *J. Power Sources*, **262**, 129 (2014).
23. K. A. Murashko, J. Pyrhönen, and J. Jokiniemi, *Int. J. Heat Mass Transf.*, **162**, 120330 (2020).
24. D. Bernardi, *J. Electrochem. Soc.*, **132**, 5 (1985).
25. M. Wetjen, D. Pritzl, R. Jung, S. Solchenbach, R. Ghadimi, and H. A. Gasteiger, *J. Electrochem. Soc.*, **164**, A2840 (2017).
26. S. Chae, S. Choi, N. Kim, J. Sung, and J. Cho, *Angew. Chemie Int. Ed.*, **59**, 110 (2020).
27. D. Allart, M. Montaru, and H. Gualous, *J. Electrochem. Soc.*, **165**, A380 (2018).